HHS Public Access

Author manuscript

Neuron. Author manuscript; available in PMC 2016 March 04.

Published in final edited form as:

Neuron. 2015 March 4; 85(5): 1043–1055. doi:10.1016/j.neuron.2015.02.011.

Melanopsin Tristability for Sustained and Broadband Phototransduction

Alan Joseph Emanuel[1,2,3,*] and **Michael Tri Hoang Do**[1,2,3,*]

[1]F.M. Kirby Neurobiology Center and Department of Neurology, Boston Children's Hospital and Harvard Medical School. Center for Life Science 12061, 3 Blackfan Circle, Boston, MA 02115, USA

[2]Center for Brain Science, Harvard University, Cambridge, MA 02138, USA

[3]Division of Sleep Medicine, Brigham and Women's Hospital and Harvard Medical School, Boston, MA, 02115, USA

SUMMARY

Mammals rely upon three ocular photoreceptors to sense light: rods, cones, and intrinsically photosensitive retinal ganglion cells (ipRGCs). Rods and cones resolve details in the visual scene. Conversely, ipRGCs integrate over time and space, primarily to support "non-image" vision. The integrative mechanisms of ipRGCs are enigmatic, particularly since these cells use a phototransduction motif that allows invertebrates like *Drosophila* to parse light with exceptional temporal resolution. Here, we provide evidence for a single mechanism that allows ipRGCs to integrate over both time and wavelength. Light distributes the visual pigment, melanopsin, across three states, two silent and one signaling. Photoequilibration among states maintains pigment availability for sustained signaling, stability of the signaling state permits minutes-long temporal summation, and modest spectral separation of the silent states promotes uniform activation across wavelengths. By broadening the tuning of ipRGCs in both temporal and chromatic domains, melanopsin tristability produces signal integration for physiology and behavior.

INTRODUCTION

The visual system resolves detail to support familiar tasks like recognizing objects and guiding action, but many processes have quite different requirements for sensing light. These "non-image" visual functions include the regulation of sleep, hormone levels, pupil contraction, and the circadian clock (reviewed by Do and Yau, 2010; Lucas et al., 2014).

*Correspondence should be addressed to aemanuel@fas.harvard.edu or michael.do@childrens.harvard.edu.

AUTHOR CONTRIBUTIONS

A.J.E. and M.T.H.D. designed experiments, which were conducted by A.J.E., and wrote the paper.

A.J.E. and M.T.H.D. have no conflicts of interest.

They tend to integrate rather than resolve, thereby smoothing fluctuations in light level across space and time to produce accurate representations of overall irradiance. The degree of integration can be remarkable. For instance, the circadian clock responds similarly to a given number of photons whether that number is delivered over milliseconds or minutes (Nelson and Takahashi, 1991). The clock uses irradiance to synchronize its endogenous rhythm with the solar day, thereby establishing normal patterns of gene expression in practically every tissue and allowing organisms to anticipate cycles of key parameters such as temperature and predator behavior (Mohawk et al., 2012). Dysregulation of the clock is linked to psychiatric illness, cardiovascular disease, metabolic disorders, and cancer (Takahashi et al., 2008).

Mammalian non-image vision begins in the retina and is supported by intrinsically photosensitive retinal ganglion cells (ipRGCs; Berson et al., 2002). IpRGCs are like conventional retinal ganglion cells (RGCs) in that they convey visual information to the brain that originates from the rod and cone photoreceptors. IpRGCs also sense light directly through their own mechanism of phototransduction. Selective elimination of ipRGC phototransduction has broad effects on the organism. Some visual functions are unable to reach their natural maxima. For instance, pupil constriction and circadian phase-shifting cannot be driven to completion; instead, they saturate at abnormally low light intensities (Lucas et al., 2003; Panda et al., 2002). Furthermore, some functions are abnormally fleeting. For example, pupil constriction and the acute modulation of locomotor activity are not sustained during steady illumination (Mrosovsky and Hattar, 2003; Zhu et al., 2007). Thus, ipRGC phototransduction appears to be particularly important at high light intensities (i.e., room light and above) and over extended time scales (i.e., seconds to hours).

IpRGCs sense light using a visual pigment called melanopsin (Provencio et al., 1998; Provencio et al., 2000). The wavelength sensitivity of melanopsin is precisely mirrored by that of ipRGCs, expression of melanopsin is required for all intrinsic light responses in ipRGCs, and heterologous expression of melanopsin in other cell types renders them photosensitive with the known characteristics of melanopsin (Berson et al., 2002; Dacey et al., 2005; Hattar et al., 2003; Lucas et al., 2003; Melyan et al., 2005; Panda et al., 2005; Qiu et al., 2005). Melanopsin is unusual in that it is expressed in vertebrates but is most homologous to the rhabdomeric pigments that are typically found in invertebrates (Provencio et al., 1998; Provencio et al., 2000; Shichida and Matsuyama, 2009). Within ipRGCs, melanopsin drives a transduction cascade that is distinguished by its prolonged time course. For example, the unitary (i.e., single-photon) response of ipRGC phototransduction has an integration time of eight seconds, which is approximately 300-fold longer than that of *Drosophila* photoreceptors, 100-fold longer than that of mammalian cones, and 20-fold longer than that of mammalian rods (Do et al., 2009; Henderson et al., 2000). Thus, melanopsin function appears tailored to the integrative nature of non-image vision.

We have investigated signal integration by ipRGCs and obtained evidence that it is greater than previously appreciated. Not only does the intrinsic light response integrate over minutes of time, it also integrates over wavelength. Furthermore, such integration appears to arise

from molecular properties of melanopsin that have not been found in any other native visual pigment.

RESULTS

IpRGCs Generate a Persistent Response that Produces Temporal Integration

Using established techniques, we identified ipRGCs within the *in vitro* mouse retina and monitored the output of individual neurons using the perforated-patch mode of electrophysiological recording, which preserves the melanopsin-driven light responses of these cells (Do et al., 2009; Do and Yau, 2013; Xue et al., 2011). Our principal focus was the M1 subtype of ipRGC, which is strictly required for photoregulation of the circadian clock and influences other non-image visual functions (Güler et al., 2008; Hatori et al., 2008). M1 ipRGCs are strongly driven by a melanopsin-mediated response that is ten-fold greater in sensitivity and saturated amplitude than that of other subtypes (Ecker et al., 2010; Schmidt and Kofuji, 2009, 2011). Such responses allow for precise, quantitative analysis. We recognized M1 ipRGCs by standard criteria (Experimental Procedures; Do et al., 2009; Do and Yau, 2013; Xue et al., 2011) and will refer to them simply as “ipRGCs” unless otherwise noted.

We recorded from single ipRGCs near body temperature (35 ± 1 °C) with synaptic transmission intact. We stimulated ipRGCs with xenon light, which has a spectrum that resembles sunlight, at intensities within the physiological range. During illumination, ipRGCs generated a response in which synaptic and intrinsic components were often discernable, as expected from prior studies (Perez-Leon et al., 2006; Schmidt and Kofuji, 2009; Wong et al., 2007). Upon cessation of illumination, we observed that the response could persist for many minutes in darkness.

To evaluate the ability of these persistent responses to support temporal integration, we stimulated ipRGCs successively with pulses of light (10-sec duration; intensity of 2.0×10^{-6} or 2.5×10^{-5} μW μm^{-2}, equivalent to 2.6×10^{3} or 3.3×10^{4} lux, respectively) that were separated by extended intervals of darkness (40 sec). An example of temporal integration is illustrated in Figures 1A and 1B: The persistent response increases across stimuli until reaching saturation, both at the level of spiking and the subthreshold membrane voltage (observed in 6 cells; Figure 1C). Some ipRGCs did not display temporal integration because their persistent responses were small or were already saturated with the first stimulus (n = 9 cells). Such variation in photosensitivity is expected of ipRGCs, even within the M1 subtype (Do et al., 2009; Do and Yau, 2013; Xue et al., 2011). Indeed, altering the light intensity to change the magnitude of the persistent response could unmask temporal integration in such cases (n = 2 of 2 cells tested; Figure S1).

We estimated the lifetime of the persistent response by monitoring the subthreshold membrane voltage following illumination. The decay was well-described by a single exponential with a time constant of 122 ± 34 sec (mean ± SEM, n = 10 cells with saturated persistent responses; example in Figure 1D). Thus, the persistent response is expected to promote temporal integration in a window of ~5 min, which is unexpectedly long because

the unitary response of ipRGCs decays with a time constant of 8.3 ± 1.0 sec (inferred from the dim-flash response of 18 cells measured in voltage clamp; Experimental Procedures).

The Persistent Response Arises from Melanopsin Phototransduction

To investigate the mechanism of the persistent response, we stimulated ipRGCs with monochromatic light (440–480 nm; Figure S2) near the peak wavelength sensitivity (λ_{max}) of melanopsin while isolating the intrinsic response by blocking synaptic transmission. A persistent response was produced in every case, indicating that it is inherent to ipRGCs (n = 85 cells). In current clamp, the persistent response was evident as a depolarization of the analog membrane voltage. With regard to spikes, this depolarization drove tonic firing in the largest fraction of ipRGCs, was too small to do so in others, and was so large in the remainder that spikes were attenuated (n = 18, 5, and 13 cells, respectively, probed with the same saturating pulse of short-wavelength light; Figure S2). When measured at room temperature, the persistent depolarization only decayed slightly in darkness (observation period as long as 20 min; example in Figure 2A). Near body temperature, it lasted for minutes (n = 4 cells), as expected from experiments with synaptic transmission intact (Figure 1). Surprisingly, the persistent response was acutely decreased by light—provided that this light was of a longer wavelength than the preceding, activating stimulus (Figures 2A–2D; n = 4 and 81 cells at 35 and 23 °C, respectively). Indeed, the persistent response was repeatedly increased and decreased in magnitude with successive pulses of light in a wavelength-dependent manner (Figures 2B–2D).

Together with melanopsin phototransduction, voltage-gated ion channels produce the intrinsic excitability of ipRGCs. The persistent response does not require these channels because it was neither increased nor decreased following pulses of depolarizing or hyperpolarizing current injection, respectively (all 36 cells tested). Furthermore, even when the membrane voltage was clamped, a robust persistent current was observed (n = 56 cells at −80 mV; example in Figure 3A). Comparison of persistent responses measured in current and voltage clamp (Figures 2B and 3A, respectively) indicates that phototransduction establishes a plateau of depolarization upon which voltage-gated channels primarily serve to drive action potentials.

We used voltage-clamp recording to evaluate the dependence of the persistent response on wavelength (Figure 3B; Supplemental Experimental Procedures). While all tested wavelengths activated ipRGCs during the period of illumination itself, the persistent response was largest following the shortest wavelength and smaller following longer wavelengths (Figure 3C). The noise accompanying the persistent response, which resembles that generated by melanopsin phototransduction during illumination (Do and Yau, 2013), was similarly graded with wavelength (Figure 3C). Because light must act through melanopsin to influence ipRGCs (in the absence of synaptic transmission; Lucas et al., 2003), these data indicate that ongoing activity of melanopsin underlies the persistent response.

Melanopsin Activates from Two Silent States in IpRGCs

While the persistent response has no homolog in vertebrate rods and cones, it does resemble a feature displayed by many invertebrate photoreceptors, the “prolonged depolarizing afterpotential” (PDA; Hillman et al., 1983). The PDA is prolonged because the rhabdomeric type of visual pigment used by such photoreceptors has a stable signaling state. The pigment can be repeatedly switched between its signaling state and silent state by light, thereby activating and deactivating the PDA (Hillman et al., 1983). Such bistability has long been speculated to be a property of mammalian melanopsin (Melyan et al., 2005; Mure et al., 2009; Mure et al., 2007; Panda et al., 2005), though the topic is controversial (reviewed by Schmidt et al., 2011).

A defining feature of a bistable pigment is its activation from a single conformational state, and we tested whether this is true of melanopsin in ipRGCs. A pigment state can be defined by its spectral sensitivity, which is described by a mathematical nomogram whose only free parameter is the λ_{max} (Govardovskii et al., 2000). The spectral sensitivity of a pigment state is conferred upon the photoreceptor to give the cellular action spectrum (e.g., Govardovskii et al., 2000; Hillman et al., 1983; Makino et al., 1999). Electrophysiological measurement of the action spectrum is generally more sensitive, by orders of magnitude, than biochemical measurements of the absorption spectrum (Govardovskii et al., 2000). The sensitivity afforded by electrophysiology is particularly important for delineating the properties of native melanopsin because this pigment is expressed sparsely in ipRGCs (Do et al., 2009) and these cells are few in number (Berson et al., 2010; Ecker et al., 2010).

We measured the ipRGC action spectrum under two conditions: dark adaptation (no activation) and atop a background light of 600 nm (a wavelength that minimizes the persistent response). We found that the action spectrum of dark-adapted ipRGCs was described by a single-state nomogram with a λ_{max} of 471 ± 2 nm (n = 6 cells; Figure 4), comparable to most prior reports (Lucas et al., 2014). With the 600-nm background light, the action spectrum was again described by a single-state nomogram (Figure 4). Unexpectedly, this nomogram was blue-shifted to have a λ_{max} of 453 ± 1 nm (n = 6 cells; same cells as above), which indicates the presence of a pigment state that is distinct from that observed in darkness. We observed this spectral shift in each cell tested (n = 4 cells at 35 °C and 2 cells at 23 °C with no detectable variation with temperature; λ_{max} differs between darkness and 600-nm background light with $p < 0.001$). A pulse of long-wavelength conditioning light was also effective in producing the blue-shifted pigment state (Figure S3). These experiments indicate that melanopsin activates from more than one state and is therefore not bistable.

When we delivered a background of 440-nm light (a wavelength that produces a large persistent response), ipRGCs exhibited an action spectrum that is broader than that of a single pigment state. Rather, it is described by the weighted sum of the 471-nm (69 ± 7%) and 453-nm (31 ± 7%) nomograms (n = 4 cells at 23 °C; Figure 5A). To test the effect of all visible wavelengths, we used a background of xenon light (1.5×10^{-7} μW μm^{-2}, equivalent to 50 lux, an intensity similar to dim room light). Again, ipRGCs displayed an action spectrum that was described by the weighted sum of the 471-nm (59 ± 8%) and 453-nm (41± 8%) nomograms (n = 5 cells at 35 °C and 4 cells at 23 °C with no detectable variation

with temperature; Figure 5B). Collectively, these data suggest that the ipRGC action spectrum reflects one pigment state, another, or both depending on illumination conditions (Figures 4 and 5). In other words, melanopsin activates from two states, which we refer to as cyan (λ_{max} = 471 nm) and violet (453 nm).

Uniformity of Phototransduction Evoked from Two Silent States of Melanopsin

To determine whether ipRGCs respond differently to photon absorption by the cyan and violet states, we generated a dominant fraction of the violet state or a majority fraction of the cyan state using background lights (600 and 440 nm, respectively; Figures 4 and 5A) and probed transduction with dim flashes (480 nm; Figure 6A). We calibrated the intensities of the backgrounds to produce a comparable level of activation, and thus adaptation, in ipRGCs (Supplemental Experimental Procedures; Do and Yau, 2013; Wong et al., 2005). Without such calibration, differences in the responses could arise from a difference in adaptation rather than the identity of the pigment state. This consideration also precluded us from using darkness for comparison with the long-wavelength background—although darkness yields a pure cyan state, it produces no adaptation. Dim-flash responses evoked on these backgrounds had indistinguishable sensitivities and kinetics (Figures 6B and 6C). Comparing 440- and 600-nm backgrounds, sensitivities were $1.1 \pm 0.3\times10^{-6}$ versus $1.0 \pm 0.3\times10^{-6}$ pA photon^{-1} μm^2 (p = 0.56), while time constants were 1.4 ± 0.3 versus 1.6 ± 0.2 sec (τ_1 of a fit using the convolution of two exponentials; p = 0.36) and 8.7 ± 2.8 versus 7.5 ± 1.3 sec (τ_2; p = 0.52, n = 5 cells). Thus, we did not detect a dependence of downstream signaling on silent states. Equivalent activation from the cyan and violet states, which are separated by ~20 nm, broadens the wavelength tuning of ipRGCs. Although modest, this spectral separation is comparable to that between the red (λ_{max} = 552 nm) and green (530 nm) cone pigments that serves human color vision (Merbs and Nathans, 1992). Here, this separation exists within a single pigment.

Photoequilibrium of Melanopsin States Supports Temporal and Chromatic Integration

Our experiments suggest the following new view of melanopsin function in the mammalian retina. Dark-adapted ipRGCs contain melanopsin in the cyan state (Figure 4). Light produces an equilibrium of cyan, violet, and signaling “meta” states. The photoequilibrium fractions of these states are determined by their spectral sensitivities and the wavelength of illumination. Photon absorption by one state causes it to isomerize to another. Therefore, short wavelengths produce a photoequilibrium that favors the meta state (λ_{max} = 476 nm; Matsuyama et al., 2012) because it absorbs these wavelengths less effectively than the cyan (471 nm) and violet (453 nm) states. On the other hand, long wavelengths produce a photoequilibrium with a dominant violet state, because this state absorbs long wavelengths least effectively. The violet state is electrically silent, or largely silent, since it is formed by wavelengths that decrease ipRGC activity (Figures 2 and 3) and its isomerization activates ipRGCs (Figures 4 and 6). Thus, our biophysical measurements indicate that native melanopsin is tristable, possessing two silent states and one signaling state.

This view is inconsistent with biochemical experiments on melanopsin (Koyanagi et al., 2005; Newman et al., 2003; Shirzad-Wasei et al., 2013; Walker et al., 2008) with the exception of a study by Shichida and colleagues (Matsuyama et al., 2012). This study

demonstrated that melanopsin's ground state ("melanopsin," λ_{max} = 467 nm, containing 11-*cis* retinal) photoequilibrates with the signaling state ("metamelanopsin," 476 nm, all-*trans* retinal). There was also evidence of photoequilibration between metamelanopsin and a third state, called "extramelanopsin" (446 nm) that contained 7-*cis* retinal. In other words, melanopsin ⇋ metamelanopsin ⇋ extramelanopsin, with direct conversion between melanopsin and extramelanopsin neither detected nor expected due to energetic constraints (Matsuyama et al., 2012). A physiological role for extramelanopsin was considered hypothetical because pigments containing 7-*cis* retinal have not been thought to exist in nature (Matsuyama et al., 2012; Sekharan and Morokuma, 2011) and these biochemical experiments were performed under highly reduced conditions (e.g., truncated pigment was expressed heterologously, solubilized in detergent, and tested at 0 °C). Nevertheless, the spectrum of extramelanopsin closely resembles that of the violet state we observe in ipRGCs (λ_{max} = 446 nm and 453 nm, respectively; Figure S4).

To make this comparison between melanopsin biochemistry and ipRGC physiology quantitative, we developed a numerical model that uses parameters measured from purified melanopsin to predict the photoequilibrium of pigment states arising from any excitation spectrum (Experimental Procedures; Figures 7A and S4; Matsuyama et al., 2012). The model predicts that short wavelengths drive most pigment into the metamelanopsin ("M") state, which parallels our experimental finding that these wavelengths generate the largest persistent responses (which reflect the M-like meta state; Figure 3). The remaining pigment is predicted to be divided between the melanopsin ("R") and extramelanopsin ("E") states (Figure 7B). For example, at 440 nm, the E state should compose 46% of the silent states. Our experiments on ipRGCs are in general agreement: Illumination at this wavelength produces a photoequilibrium in which ~31% of the pigment occupies the E-like violet state (Figure 5A). For long wavelengths, the model predicts that there is a small fraction of the M and R states as well as a large fraction of the E state (Figure 7B), which accords with our observation that these wavelengths produce the smallest persistent responses in ipRGCs (Figures 2 and 3). At 600 nm, the E state is predicted to account for 92% of the silent states. When delivered to ipRGCs, light of this wavelength produces a photoequilibrium in which the only detectable silent state is the E-like violet state (Figure 4 and Experimental Procedures). Thus, mammalian melanopsin appears to be tristable in its native environment as well as when purified, and tristability can account for the integrative properties of ipRGCs that we observe.

Tristability Confers Unique Properties to Melanopsin

To investigate how tristability operates under diverse illumination conditions, we assessed model outputs for common light sources (Figure 8A; Johnsen et al., 2006). Remarkably, despite having diverse spectra, these sources are predicted to have practically identical effects on the photoequilibrium of melanopsin states, resembling monochromatic short-wavelength light in producing a majority fraction of the M state and roughly even fractions of the R and E states (Figure 8B).

We generated two additional models to compare the properties of tristable and bistable visual pigments. The first is a hypothetical, "bistable melanopsin" that lacks the E state

(Figure 8C) and the second is *Drosophila* rhodopsin (Figure 8D). All relevant biochemical parameters are known for both models (Matsuyama et al., 2012; Ostroy, 1978; Stavenga, 2010). The principal difference between these bistable models is that the spectral sensitivities of the ground and signaling states are similar for melanopsin (λ_{max} = 467 and 476 nm, respectively) but different for rhodopsin (480 and 570 nm). We find that the photoequilibrium of bistable melanopsin, but not of rhodopsin, displays a high degree of invariance across diverse lighting spectra. By contrast, the photoequilibrium of rhodopsin, but not of bistable melanopsin, can have a nearly pure fraction of either the silent state or the signaling state. Tristable melanopsin is distinct from bistable pigments in that it displays both spectral invariance and state purity (Figure 8B). Furthermore, the approach of tristable melanopsin to photoequilibrium is slower than that of bistable melanopsin or *Drosophila* rhodopsin (by 1.6- and 6.1-fold, respectively), consistent with the integrative nature of non-image vision.

DISCUSSION

We have found that phototransduction in ipRGCs exhibits a high degree of signal integration that is consistent with the characteristics of non-image vision. Melanopsin activity generates persistent responses that support temporal integration over many minutes. We know of no other sensory cell that exhibits such a high degree of temporal integration; notably, ipRGCs accomplish this integration with signaling components that are employed in other systems to resolve signals on a millisecond time scale (e.g., Henderson et al., 2000). Furthermore, the persistent responses of ipRGCs are activated by a wider range of wavelengths than expected from a single visual pigment (Govardovskii et al., 2000). We have provided evidence that this chromatic integration reflects activation of melanopsin from two spectrally distinct silent states, which we have called cyan and violet (Figure S5).

The violet state of melanopsin resembles the E state that Shichida and colleagues defined biochemically for purified melanopsin (Matsuyama et al., 2012). The E state is unusual in using 7-*cis* retinal, a chromophore that has not yet been found in visual pigments under natural conditions. Molecular dynamics simulations have predicted that 7-*cis* retinal would produce an inactive pigment (Sekharan and Morokuma, 2011). Therefore, like the violet state, the E state is expected to be silent. Moreover, rhodopsins experimentally reconstituted with 11-*cis* or 7-*cis* retinal differ in the initial stages of photoactivation but converge before G-protein engagement (Shichida et al., 1991). This is consistent with our observation of indistinguishable activation from the cyan and violet states in ipRGCs (Figure 6). Thus, extramelanopsin and the violet state are likely to be one and the same. Purification of 7-*cis* retinal from ipRGCs would provide a confirmation of this idea, though such experiments are challenging due to the miniscule amount of melanopsin in the retina (Berson et al., 2010; Do et al., 2009; Ecker et al., 2010). Such confirmation would motivate investigation of how melanopsin forms this isomer naturally while other pigments require artificial conditions (Azuma and Azuma, 1985; Maeda et al., 1978; Maeda et al., 1979); intriguingly, simulations already suggest that retinal has a distinct geometry when bound within melanopsin (Sekharan et al., 2012).

Some studies have suggested that mammalian melanopsin has only one silent state and is bistable (Melyan et al., 2005; Mure et al., 2009; Mure et al., 2007; Panda et al., 2005; Shirzad-Wasei et al., 2013). Other studies have not detected any photoequilibration of melanopsin among stable states (Do et al., 2009; Fu et al., 2005; Mawad and Van Gelder, 2008; Qiu et al., 2005; Sexton et al., 2012). Much of this controversy may stem from properties of tristability that we have described here. The largest persistent responses we observe are approximately 30 pA and most are <10 pA, which can be difficult to detect. These responses are also associated with decreases in input resistance and photosensitivity (Figures 2C and 3A), which are typical criteria for terminating a recording session (Do et al., 2009; Do and Yau, 2013). Finally, even though persistent currents are small, they often can drive ipRGCs into depolarization block due to the high input resistance of these cells (Figure 2C; Do et al., 2009; Do and Yau, 2013; Schmidt and Kofuji, 2009); these activated but weakly- or non-spiking cells would not be apparent in extracellular recordings (Mawad and Van Gelder, 2008; Sexton et al., 2012).

Our results suggest another reason that melanopsin's nature has been elusive. The signaling state exhibits a monotonic decline in absolute sensitivity with increasing wavelength (past its λ_{max} of ~480 nm), which makes longer wavelengths less effective at depopulating it. On the other hand, the relative sensitivities of the three states are such that wavelengths near 600 nm are best for selectively depopulating the signaling state (Figure S4D). The optimal wavelength of cellular deactivation should reflect a balance of these absolute and relative sensitivities. Indeed, this optimal wavelength appears to be ~580 nm in our hands. A comparable optimum was deduced from behavioral experiments (Mure et al., 2009) and has been interpreted as the λ_{max} of a bistable melanopsin's signaling state. Our data indicate that it is, instead, a consequence of melanopsin tristability. Notably, even light of the optimal wavelength must be intense or prolonged to produce an acute decrease of the persistent response, because all states of melanopsin absorb long wavelengths poorly.

With regard to the spectral sensitivity of melanopsin activation, reported λ_{max} values range from ~420 nm to ~480 nm in studies conducted at biochemical, cellular, and behavioral levels (e.g., Berson et al., 2002; Brainard et al., 2001; Lucas et al., 2001; Matsuyama et al., 2012; Melyan et al., 2005; Newman et al., 2003; Panda et al., 2005; Qiu et al., 2005). The existence of the violet state helps explain this dispersion in values because its contribution to the observed spectral sensitivity can vary with illumination conditions; it is present during illumination and absent following prolonged darkness.

Melanopsin tristability appears to have advantages for non-image vision. First, photoequilibration of melanopsin among signaling and silent states supports the sustained activity of ipRGCs by maintaining the availability of pigment molecules for activation. By contrast, the monostable rod and cone pigments spontaneously dissociate into opsin and chromophore after a single activation, thereby losing photosensitivity. Because pigment regeneration requires a slow series of reactions that takes place in accessory cells, rods and cones have limited intrinsic capacities for sustained signaling (Wang and Kefalov, 2011). Our observations of the violet state and its activation provide evidence for light-driven regeneration of melanopsin in ipRGCs. Such regeneration may be particularly important to ipRGCs because they express relatively few melanopsin molecules (Do et al., 2009) yet

must capture photons continuously over the long time scales of non-image visual responses (Mrosovsky and Hattar, 2003; Wong, 2012).

With regard to sustaining photon capture, tristability is not expected to differ from bistability, which raises the question of whether tristability provides unique advantages. Our work indicates that tristable melanopsin displays an activation level that is similar across a variety of broadband spectra ("spectral invariance") and can range from a small minimum to a large maximum ("state purity"). By contrast, a bistable pigment can display either spectral invariance or state purity—depending on the relative wavelength sensitivity of its two states—but not both. State purity facilitates the fine-tuning of pigment function to behavioral needs. For example, the balance between activation and deactivation can be flexibly altered through the expression of screening pigments that are upstream of the photoreceptors, a strategy that is used by many species for adaptation to diverse habitats (Cronin et al., 2001; Hardie and Postma, 2008). Tristable melanopsin has two additional features that distinguish it from bistable pigments. First, its spectral sensitivity is broadened by activation from two silent states, which confers a moderate degree of wavelength integration. Second, tristable melanopsin approaches photoequilibrium with an extended time course, which imposes a low-pass filter on visual signals. Thus, tristability endows melanopsin signaling with a unique set of properties that is consistent with the integrative nature of non-image vision.

A noteworthy implication of our study is that light cannot produce a pure population of melanopsin's ground state. Nevertheless, this is the only state detected in dark-adapted ipRGCs biochemically (Sexton et al., 2012; Walker et al., 2008) and in our own biophysical experiments (Figure 4). Therefore, melanopsin is likely to return to the ground state through a light-independent mechanism. We expect such dark regeneration to be slow because the persistent response (reflecting the meta state) can be observed for many minutes following its induction by light, and the action spectra of ipRGCs (reflecting the fractional occupancy of cyan and violet states) agree with predictions from our state model, which only includes light-driven transitions. Melanopsin can be regenerated by the administration of exogenous chromophore (Do et al., 2009; Fu et al., 2005), at least in some circumstances (Sexton et al., 2012), which raises the possibility that formation of the ground state involves bleaching and regeneration.

In summary, ipRGCs respond to common lighting conditions by producing signals that sum over minutes, regenerating melanopsin molecules from the signaling state, and expanding their spectral sensitivity. We have presented evidence that these properties share a common origin in melanopsin tristability; namely, the photoequilibration of melanopsin among silent cyan, silent violet, and signaling meta states. It is presently unknown if tristability is unique to mammalian melanopsin or is also a property of other visual pigments. Regardless, melanopsin tristability imparts broadband and sustained signals to the many processes that have been ascribed to ipRGCs, from neural and vascular development (Rao et al., 2013; Renna et al., 2011) to the regulation of mood and the circadian clock (reviewed by Do and Yau, 2010; Lucas et al., 2014). Tristability is also expected to increase the integrative capacity of cells that are rendered photosensitive through the optogenetic use of melanopsin, and permit these cells to be acutely deactivated with long-wavelength light (Lin et al., 2008; Ye et al., 2011).

EXPERIMENTAL PROCEDURES

Detailed procedures for individual experiments are included in Supplemental Experimental Procedures.

Tissue

All procedures were approved by the Institutional Animal Care and Use Committee of Boston Children's Hospital. BAC-transgenic mice (either sex, P20–140, housed in a 12-h light/12-h dark cycle) with ipRGCs labeled by expression of tdTomato from the melanopsin gene locus, were used (Do et al., 2009). Mice were dark-adapted for >1.5 h and experiments were performed between zeitgeber times 3 and 10 (where 0 is lights on). Under dim red light, animals were anesthetized with Avertin, enucleated, and euthanized. The retina was mechanically freed from the retinal pigment epithelium and vitreous humor in carbogenated Ames' medium (i.e., equilibrated with 95% O_2/5% CO_2). The retina was flattened with peripheral cuts and held in the recording chamber, photoreceptors down, by a platinum-iridium frame strung with lycra fibers or a coverslip coated with poly-L-lysine.

Electrophysiology

The flat-mount retina was superfused with carbogenated Ames' medium at ~5 ml/min on the stage of an upright microscope. Cells were viewed with differential interference contrast optics using infrared transillumination (850-nm center wavelength and 30-nm width at half maximum). IpRGCs were visualized with ~1 s of light (25-nm bandpass centered on 545 nm, 1×10^{10} photons μm^{-2} s^{-1}; Figure S2) and the overlying inner limiting membrane was mechanically removed. Cells were dark-adapted for >15 min before data were collected. Pipettes (2–6 MΩ) were wrapped with parafilm to reduce capacitance. Series resistance (generally ≤ 50 MΩ) was monitored. Integrity of the perforated-patch configuration was tested with periodic test flashes and, in some cases, brief visualization of lucifer yellow (which does not permeate amphotericin B) at the end of the experiment. Recordings were performed near physiological temperature (35 ± 1 °C) or, for additional stability, at room temperature (~23° C). Temperature was monitored with a thermistor in the recording chamber. Recordings were low-pass filtered at 4–10 kHz (current clamp) or 2 kHz (voltage clamp) and sampling exceeded the Nyquist minimum. Analysis was performed using Clampfit and Igor Pro. Nearly all ipRGCs we recorded are likely to be of the M1 subtype based on their bright tdTomato labeling; large intrinsic light responses (typically >100 pA); wide, highly-accommodating action potentials; and, often, dendrites that could be seen extending into the inner plexiform layer (Do et al., 2009; Do and Yau, 2013; Ecker et al., 2010; Schmidt and Kofuji, 2009; Xue et al., 2011). The few apparently non-M1 ipRGCs encountered were not overtly different with regard to melanopsin tristability, exhibiting persistent responses to short-wavelength light and shifted action spectra during or after long-wavelength light. Solutions are detailed in Supplemental Experimental Procedures.

Optical Stimulation

Light from 75-W xenon arc lamps or a 100-W mercury halide lamp was filtered to deplete heat while selecting intensity and wavelength. Delivery through a 40X objective produced a uniform field (480-μm diameter) centered on the soma. Electromechanical shutters

controlled stimulus timing. Light stimuli were measured at the site of the preparation using a calibrated radiometer and spectrometer. Light delivered through 10-nm bandpass filters were assumed to be of the center wavelength; for broader filters, photon flux was calculated from measured spectra (Figures 8 and S2). Photometric units were calculated using the CIE standard photopic luminosity function (Sharpe et al., 2005). “Flashes” are impulse stimuli (i.e., duration and intensity can be interchanged to give the same response).

Numerical Model of Melanopsin Tristability

The distribution of biochemically-defined melanopsin states (Matsuyama et al., 2012) as a function of wavelength was estimated with a numerical simulation in which occupancy of each state is calculated with each time step. The states are melanopsin (R), metamelanopsin (M), and extramelanopsin (E). A state depopulates if a molecule in that state absorbs a photon and isomerizes (thus converting to another state). A state populates if a molecule in an adjoining state absorbs a photon and isomerizes. R and E both interconvert directly with M but not each other, in accordance with biochemical data on purified melanopsin (Matsuyama et al., 2012) and the likelihood, given energetic constraints, that the transition from one *cis* isoform to another occurs via the all-*trans* conformation. For each state, photon absorption is governed by the extinction coefficient (ε, in units of $cm^2\ mol^{-1}$), which has a spectral dependence, $A(\lambda)$. Following photon absorption, the probability of isomerization is given by the quantum efficiency (φ). The equations are

$$f_{n+1}^{R}=f_{n}^{R}+f^{M\to R}[\ln(10)\times I(\lambda)\times f_{n}^{M}\times\varepsilon_{\mathrm{M}}\times \mathrm{A}_{\mathrm{M}}(\lambda)\times\phi_{\mathrm{M}}]-[\ln(10)\times I(\lambda)\times f_{n}^{R}\times\varepsilon_{\mathrm{R}}\times \mathrm{A}_{\mathrm{R}}(\lambda)\times\phi_{\mathrm{R}}]$$
$$f_{n+1}^{M}=f_{n}^{M}+[\ln(10)\times I(\lambda)\times f_{n}^{R}\times\varepsilon_{\mathrm{R}}\times \mathrm{A}_{\mathrm{R}}(\lambda)\times\phi_{\mathrm{R}}]+[\ln(10)\times I(\lambda)\times f_{n}^{E}\times\varepsilon_{\mathrm{E}}\times \mathrm{A}_{\mathrm{B}}(\lambda)\times\phi_{\mathrm{E}}]$$
$$-[\ln(10)\times I(\lambda)\times f_{n}^{M}\times\varepsilon_{\mathrm{M}}\times \mathrm{A}_{\mathrm{M}}(\lambda)\times\phi_{\mathrm{M}}]$$
$$f_{n+1}^{E}=f_{n}^{E}+f^{M\to E}[\ln(10)\times I(\lambda)\times f_{n}^{M}\times\varepsilon_{\mathrm{M}}\times \mathrm{A}_{\mathrm{M}}(\lambda)\times\phi_{\mathrm{M}}]-[\ln(10)\times I(\lambda)\times f_{n}^{E}\times\varepsilon_{\mathrm{E}}\times \mathrm{A}_{\mathrm{E}}(\lambda)\times\phi_{\mathrm{E}}]$$

where f^R, f^M, and f^E are the fractional occupancies of each state and sum to 1. We typically begin our simulation with $f_0^R=1$, reflecting dark adaptation but the equilibrium state is insensitive to the initial conditions. $f^{M\to R}$ is the fraction of M isomerizations that yields R and $f^{M\to E}$ is the fraction that yields E; $f^{M\to R}+f^{M\to E}=1$. $I(\lambda)$ is the light intensity in mol photons $cm^{-2}\ sec^{-1}\ nm^{-1}$ (higher intensities simply give faster approaches to equilibrium; Figure S4). The *ln(10)* term originates with the Beer-Lambert law governing absorbance of light. Equilibrium was defined at the point when the fraction of each state changes by $< 1.0 \times 10^{-20}$ between time steps (of at least 1 ms). For $A(\lambda)$, we use the standard spectral template for A1-based pigments, including both α and β absorption bands (Govardovskii et al., 2000), with the λ_{max} values reported for purified, mammalian melanopsin (R = 467 nm, M = 476 nm, and E = 446 nm; Matsuyama et al., 2012).

All model parameters except for φ_E and $f^{M\to R}$ (thus also $f^{M\to E}$) have been defined by Shichida and colleagues (Matsuyama et al., 2012). Most natural pigments have a quantum efficiency of activation near 0.7 (Dartnall, 1972); where it has been studied, the quantum efficiency of deactivation for bistable pigments is as low as 0.2 (Cronin and Goldsmith, 1982; Matsuyama et al., 2012). There is little information available on the quantum efficiency of pigments containing 7-cis retinal (Shichida et al., 1991), like the E state. For

our model, we selected a φ_E of 0.4, which is intermediate between the values for melanopsin and metamelanopsin (Matsuyama et al., 2012), and an $f^{M\to R}$ (and thus $f^{M\to E}$) of 0.5.

We do not consider light-independent transitions between states because the thermal decay of the M and E states appears to be negligible over the time scales of our experiments, especially at 23 °C. For instance, the persistent response (reflecting the signaling, or M state) is stable for minutes at 35 °C and 23 °C (Figures 1D and 2A) and the spectral sensitivity of the violet state (the physiological homolog of the biochemical E state) can be measured from ipRGCs in a >10 min window following a conditioning light that produces it (at 23 °C, Figure S3). Furthermore, many of our experiments are performed with continuous illumination, which maintains the photoequilibrium distribution of melanopsin states.

Numerical Models of Bistable Pigments

The equations that compose the models of bistable pigments are

$$f_{n+1}^{R}=f_{n}^{R}+[\ln(10)\times I(\lambda)\times f_{n}^{M}\times\varepsilon_{\mathrm{M}}\times\mathrm{A}_{\mathrm{M}}(\lambda)+\phi_{\mathrm{M}}]-[\ln(10)\times I(\lambda)\times f_{n}^{R}\times\varepsilon_{\mathrm{R}}\times\mathrm{A}_{\mathrm{R}}(\lambda)\times\phi_{\mathrm{R}}]$$
$$f_{n+1}^{M}=f_{n}^{M}+[\ln(10)\times I(\lambda)\times f_{n}^{R}\times\varepsilon_{\mathrm{R}}\times\mathrm{A}_{\mathrm{R}}(\lambda)\times\phi_{\mathrm{R}}]-[\ln(10)\times I(\lambda)\times f_{n}^{M}\times\varepsilon_{\mathrm{M}}\times\mathrm{A}_{\mathrm{M}}(\lambda)\times\phi_{\mathrm{M}}]$$

Variables are identical to those given for the tristable melanopsin model. For the hypothetical bistable melanopsin," all values are the same as for the tristable melanopsin model. For *Drosophila* rhodopsin, ε_R = 35,000 cm^2 mol^{-1} and ε_M = 56,000 cm^2 mol^{-1} (Ostroy, 1978). φ_M has been measured to be 0.71 of φ_R (Stavenga, 2010). φ_R itself has not been directly measured but its proportionality with φ_M is sufficient for accurate prediction of photoequilibrium pigment fractions. $A_R(\lambda)$ and $A_M(\lambda)$ are Govardovskii nomograms (Govardovskii et al., 2000) with λ_{max} values of 480 and 570 nm, respectively, which fit *Drosophila* pigment states (Stavenga, 2010).

Statistical Methods

We used non-parametric statistics, employing the Mann-Whitney U test for unpaired data and the Wilcoxon signed-rank test for paired data. To compare more than two groups with repeated measures, we used the Friedman test and a post-hoc Wilcoxon signed-rank test with Bonferroni correction.

Supplementary Material

Refer to Web version on PubMed Central for supplementary material.

Acknowledgments

We thank T. Matsuyama, Y. Shichida, D.D. Oprian, R.I. Wilson, C.J. Woolf, and laboratory members (M.C. Brown, G.S. Bryman, A. Liu, and E.S. Milner) for discussions; and R. Adams, E. Egan and M. Kwiatkowski for technical assistance. This work was supported by grants from the National Science Foundation (Graduate Research Fellowship, A.J.E.), National Institutes of Health (R01 EY023648, M.T.H.D.; P30 HD18655, Boston Children's Hospital IDDRC; P30 EY012196, Harvard Medical School; and T32 HL007901, HMS Division of Sleep Medicine), the Whitehall Foundation (2011-05-15, M.T.H.D.), and The Karl Kirchgessner Foundation (M.T.H.D.).

References

Azuma K, Azuma M. Absorbance and circular dichroism spectra of 7-*cis* photoproduct formed by irradiating frog rhodopsin. Photochem Photobiol. 1985; 41:165–169. [PubMed: 3873662]

Berson DM, Castrucci AM, Provencio I. Morphology and mosaics of melanopsin-expressing retinal ganglion cell types in mice. J Comp Neurol. 2010; 518:17.

Berson DM, Dunn FA, Takao M. Phototransduction by retinal ganglion cells that set the circadian clock. Science. 2002; 295:1070–1073. [PubMed: 11834835]

Brainard GC, Hanifin JP, Greeson JM, Byrne B, Glickman G, Gerner E, Rollag MD. Action spectrum for melatonin regulation in humans: evidence for a novel circadian photoreceptor. J Neurosci. 2001; 21:6405–6412. [PubMed: 11487664]

Cronin TW, Caldwell RL, Marshall J. Sensory adaptation. Tunable colour vision in a mantis shrimp. Nature. 2001; 411:547–548. [PubMed: 11385560]

Cronin TW, Goldsmith TH. Quantum efficiency and photosensitivity of the rhodopsin equilibrium metarhodopsin conversion in crayfish photoreceptors. Photochem Photobiol. 1982; 36:447–454. [PubMed: 7146115]

Dacey DM, Liao HW, Peterson BB, Robinson FR, Smith VC, Pokorny J, Yau KW, Gamlin PD. Melanopsin-expressing ganglion cells in primate retina signal colour and irradiance and project to the LGN. Nature. 2005; 433:749–754. [PubMed: 15716953]

Dartnall, HJA. Photosensitivity. In: Dartnall, HJA., editor. Photochemistry of Vision. New York: Springer-Verlag; 1972. p. 122-145.

Do MTH, Kang SH, Xue T, Zhong H, Liao HW, Bergles DE, Yau KW. Photon capture and signalling by melanopsin retinal ganglion cells. Nature. 2009; 457:281–287. [PubMed: 19118382]

Do MTH, Yau KW. Intrinsically photosensitive retinal ganglion cells. Physiol Rev. 2010; 90:1547–1581. [PubMed: 20959623]

Do MTH, Yau KW. Adaptation to steady light by intrinsically photosensitive retinal ganglion cells. P Natl Acad Sci USA. 2013; 110:7470–7475.

Ecker JL, Dumitrescu ON, Wong KY, Alam NM, Chen SK, LeGates T, Renna JM, Prusky GT, Berson DM, Hattar S. Melanopsin-expressing retinal ganglion-cell photoreceptors: cellular diversity and role in pattern vision. Neuron. 2010; 67:49–60. [PubMed: 20624591]

Fu Y, Zhong H, Wang MH, Luo DG, Liao HW, Maeda H, Hattar S, Frishman LJ, Yau KW. Intrinsically photosensitive retinal ganglion cells detect light with a vitamin A-based photopigment, melanopsin. P Natl Acad Sci USA. 2005; 102:10339–10344.

Govardovskii VI, Fyhrquist N, Reuter T, Kuzmin DG, Donner K. In search of the visual pigment template. Visual Neurosci. 2000; 17:509–528.

Güler AD, Ecker JL, Lall GS, Haq S, Altimus CM, Liao HW, Barnard AR, Cahill H, Badea TC, Zhao H, et al. Melanopsin cells are the principal conduits for rod-cone input to non-image-forming vision. Nature. 2008; 453:102–105. [PubMed: 18432195]

Hardie, RC.; Postma, M. 1.05 – Phototransduction in microvillar photoreceptors of *Drosophila* and other invertebrates. In: Basbaum, AI., editor. The Senses: A Comprehensive Reference. Elsevier Science/Academic Press; 2008.

Hatori M, Le H, Vollmers C, Keding SR, Tanaka N, Schmedt C, Jegla T, Panda S. Inducible ablation of melanopsin-expressing retinal ganglion cells reveals their central role in non-image forming visual responses. PLoS ONE. 2008; 3:e2451. [PubMed: 18545654]

Hattar S, Lucas RJ, Mrosovsky N, Thompson S, Douglas RH, Hankins MW, Lem J, Biel M, Hofmann F, Foster RG, Yau KW. Melanopsin and rod-cone photoreceptive systems account for all major accessory visual functions in mice. Nature. 2003; 424:76–81. [PubMed: 12808468]

Henderson SR, Reuss H, Hardie RC. Single photon responses in *Drosophila* photoreceptors and their regulation by Ca^{2+} J Physiol. 2000; 524:179–194. [PubMed: 10747191]

Hillman P, Hochstein S, Minke B. Transduction in invertebrate photoreceptors: role of pigment bistability. Physiol Rev. 1983; 63:668–772. [PubMed: 6340134]

Johnsen S, Kelber A, Warrant E, Sweeney AM, Widder EA, Lee RL Jr, Hernandez-Andres J. Crepuscular and nocturnal illumination and its effects on color perception by the nocturnal hawkmoth *Deilephila elpenor*. J Exp Biol. 2006; 209:789–800. [PubMed: 16481568]

Koyanagi M, Kubokawa K, Tsukamoto H, Shichida Y, Terakita A. Cephalochordate melanopsin: evolutionary linkage between invertebrate visual cells and vertebrate photosensitive retinal ganglion cells. Curr Biol. 2005; 15:1065–1069. [PubMed: 15936279]

Lin B, Koizumi A, Tanaka N, Panda S, Masland RH. Restoration of visual function in retinal degeneration mice by ectopic expression of melanopsin. P Natl Acad Sci USA. 2008; 105:16009–16014.

Lucas RJ, Douglas RH, Foster RG. Characterization of an ocular photopigment capable of driving pupillary constriction in mice. Nat Neurosci. 2001; 4:621–626. [PubMed: 11369943]

Lucas RJ, Hattar S, Takao M, Berson DM, Foster RG, Yau KW. Diminished pupillary light reflex at high irradiances in melanopsin-knockout mice. Science. 2003; 299:245–247. [PubMed: 12522249]

Lucas RJ, Peirson SN, Berson DM, Brown TM, Cooper HM, Czeisler CA, Figueiro MG, Gamlin PD, Lockley SW, O'Hagan JB, et al. Measuring and using light in the melanopsin age. Trends Neurosci. 2014; 37:1–9. [PubMed: 24287308]

Maeda A, Ogurusu T, Shichida Y, Tokunaga F, Yoshizawa T. Formation of a 7-*cis* retinal pigment by irradiating cattle rhodopsin at low temperatures. FEBS Letters. 1978; 92:77–80.

Maeda A, Shichida Y, Yoshizawa T. Formation of 7-*cis*- and 13-*cis*-retinal pigments by irradiating squid rhodopsin. Biochemistry. 1979; 18:5.

Makino CL, Groesbeek M, Lugtenburg J, Baylor DA. Spectral tuning in salamander visual pigments studied with dihydroretinal chromophores. Biophys J. 1999; 77:1024–1035. [PubMed: 10423447]

Matsuyama T, Yamashita T, Imamoto Y, Shichida Y. Photochemical properties of mammalian melanopsin. Biochemistry. 2012; 51:5454–5462. [PubMed: 22670683]

Mawad K, Van Gelder RN. Absence of long-wavelength photic potentiation of murine intrinsically photosensitive retinal ganglion cell firing *in vitro*. J Biol Rhythms. 2008; 23:387–391. [PubMed: 18838602]

Melyan Z, Tarttelin EE, Bellingham J, Lucas RJ, Hankins MW. Addition of human melanopsin renders mammalian cells photoresponsive. Nature. 2005; 433:741–745. [PubMed: 15674244]

Merbs SL, Nathans J. Absorption spectra of human cone pigments. Nature. 1992; 356:433–435. [PubMed: 1557124]

Mohawk JA, Green CB, Takahashi JS. Central and peripheral circadian clocks in mammals. Annu Rev Neurosci. 2012; 35:445–462. [PubMed: 22483041]

Mrosovsky N, Hattar S. Impaired masking responses to light in melanopsin-knockout mice. Chronobiol Int. 2003; 20:989–999. [PubMed: 14680139]

Mure LS, Cornut PL, Rieux C, Drouyer E, Denis P, Gronfier C, Cooper HM. Melanopsin bistability: a fly's eye technology in the human retina. PLoS ONE. 2009; 4:e5991. [PubMed: 19551136]

Mure LS, Rieux C, Hattar S, Cooper HM. Melanopsin-dependent nonvisual responses: evidence for photopigment bistability *in vivo*. J Biol Rhythms. 2007; 22:411–424. [PubMed: 17876062]

Nelson DE, Takahashi JS. Sensitivity and integration in a visual pathway for circadian entrainment in the hamster (*Mesocricetus auratus*). J Physiol. 1991; 439:115–145. [PubMed: 1895235]

Newman LA, Walker MT, Brown RL, Cronin TW, Robinson PR. Melanopsin forms a functional short-wavelength photopigment. Biochemistry. 2003; 42:12734–12738. [PubMed: 14596587]

Ostroy SE. Characteristics of *Drosophila* rhodopsin in wild-type and *norpA* vision transduction mutants. J Gen Physiol. 1978; 72:717–732. [PubMed: 105082]

Panda S, Nayak SK, Campo B, Walker JR, Hogenesch JB, Jegla T. Illumination of the melanopsin signaling pathway. Science. 2005; 307:600–604. [PubMed: 15681390]

Panda S, Sato TK, Castrucci AM, Rollag MD, DeGrip WJ, Hogenesch JB, Provencio I, Kay SA. Melanopsin (*Opn4*) requirement for normal light-induced circadian phase shifting. Science. 2002; 298:2213–2216. [PubMed: 12481141]

Perez-Leon JA, Warren EJ, Allen CN, Robinson DW, Lane Brown R. Synaptic inputs to retinal ganglion cells that set the circadian clock. Eur J Neurosci. 2006; 24:1117–1123. [PubMed: 16930437]

Provencio I, Jiang G, De Grip WJ, Hayes WP, Rollag MD. Melanopsin: An opsin in melanophores, brain, and eye. P Natl Acad Sci USA. 1998; 95:340–345.

Provencio I, Rodriguez IR, Jiang G, Hayes WP, Moreira EF, Rollag MD. A novel human opsin in the inner retina. J Neurosci. 2000; 20:600–605. [PubMed: 10632589]

Qiu X, Kumbalasiri T, Carlson SM, Wong KY, Krishna V, Provencio I, Berson DM. Induction of photosensitivity by heterologous expression of melanopsin. Nature. 2005; 433:745–749. [PubMed: 15674243]

Rao S, Chun C, Fan J, Kofron JM, Yang MB, Hegde RS, Ferrara N, Copenhagen DR, Lang RA. A direct and melanopsin-dependent fetal light response regulates mouse eye development. Nature. 2013; 494:243–246. [PubMed: 23334418]

Renna JM, Weng S, Berson DM. Light acts through melanopsin to alter retinal waves and segregation of retinogeniculate afferents. Nat Neurosci. 2011; 14:827–829. [PubMed: 21642974]

Schmidt TM, Chen SK, Hattar S. Intrinsically photosensitive retinal ganglion cells: many subtypes, diverse functions. Trends Neurosci. 2011; 34:572–580. [PubMed: 21816493]

Schmidt TM, Kofuji P. Functional and morphological differences among intrinsically photosensitive retinal ganglion cells. J Neurosci. 2009; 29:476–482. [PubMed: 19144848]

Schmidt TM, Kofuji P. Structure and function of bistratified intrinsically photosensitive retinal ganglion cells in the mouse. J Comp Neurol. 2011; 519:1492–1504. [PubMed: 21452206]

Sekharan S, Morokuma K. Why 11-*cis*-retinal? Why not 7-*cis*-, 9-*cis*-, or 13-*cis*-retinal in the eye? J Am Chem Soc. 2011; 133:19052–19055. [PubMed: 22026715]

Sekharan S, Wei JN, Batista VS. The active site of melanopsin: the biological clock photoreceptor. Journal of the American Chemical Society. 2012; 134:19536–19539. [PubMed: 23145979]

Sexton TJ, Golczak M, Palczewski K, Van Gelder RN. Melanopsin is highly resistant to light and chemical bleaching *in vivo*. J Biol Chem. 2012; 287:20888–20897. [PubMed: 22547062]

Sharpe LT, Stockman A, Jagla W, Jagle H. A luminous efficiency function, V*(λ), for daylight adaptation. J Vis. 2005; 5:948–968. [PubMed: 16441195]

Shichida Y, Kandori H, Okada T, Yoshizawa T, Nakashima N, Yoshihara K. Differences in the photobleaching process between 7-*cis*- and 11-*cis*-rhodopsins: a unique interaction change between the chromophore and the protein during the lumi-meta I transition. Biochemistry. 1991; 30:5918–5926. [PubMed: 1828372]

Shichida Y, Matsuyama T. Evolution of opsins and phototransduction. Phil Trans Royal Soc Lond B Biol Sci. 2009; 364:2881–2895.

Shirzad-Wasei N, van Oostrum J, Bovee-Geurts PH, Wasserman M, Bosman GJ, DeGrip WJ. Large scale expression and purification of mouse melanopsin-L in the baculovirus expression system. Protein Expr Purif. 2013; 91:134–146. [PubMed: 23921072]

Stavenga DG. On visual pigment templates and the spectral shape of invertebrate rhodopsins and metarhodopsins. J Comp Physiol A. 2010; 196:869–878.

Takahashi JS, Hong HK, Ko CH, McDearmon EL. The genetics of mammalian circadian order and disorder: implications for physiology and disease. Nat Rev Genet. 2008; 9:764–775. [PubMed: 18802415]

Walker MT, Brown RL, Cronin TW, Robinson PR. Photochemistry of retinal chromophore in mouse melanopsin. P Natl Acad Sci USA. 2008; 105:8861–8865.

Wang JS, Kefalov VJ. The cone-specific visual cycle. Prog Retin Eye Res. 2011; 30:115–128. [PubMed: 21111842]

Wong KY. A retinal ganglion cell that can signal irradiance continuously for 10 hours. J Neurosci. 2012; 32:11478–11485. [PubMed: 22895730]

Wong KY, Dunn FA, Berson DM. Photoreceptor adaptation in intrinsically photosensitive retinal ganglion cells. Neuron. 2005; 48:1001–1010. [PubMed: 16364903]

Wong KY, Dunn FA, Graham DM, Berson DM. Synaptic influences on rat ganglion-cell photoreceptors. J Physiol. 2007; 582:279–296. [PubMed: 17510182]

Xue T, Do MTH, Riccio A, Jiang Z, Hsieh J, Wang HC, Merbs SL, Welsbie DS, Yoshioka T, Weissgerber P, et al. Melanopsin signalling in mammalian iris and retina. Nature. 2011; 479:67–73. [PubMed: 22051675]

Ye H, Daoud-El Baba M, Peng RW, Fussenegger M. A synthetic optogenetic transcription device enhances blood-glucose homeostasis in mice. Science. 2011; 332:1565–1568. [PubMed: 21700876]

Zhu Y, Tu DC, Denner D, Shane T, Fitzgerald CM, Van Gelder RN. Melanopsin-dependent persistence and photopotentiation of murine pupillary light responses. Invest Ophthalmol Vis Sci. 2007; 48:1268–1275. [PubMed: 17325172]

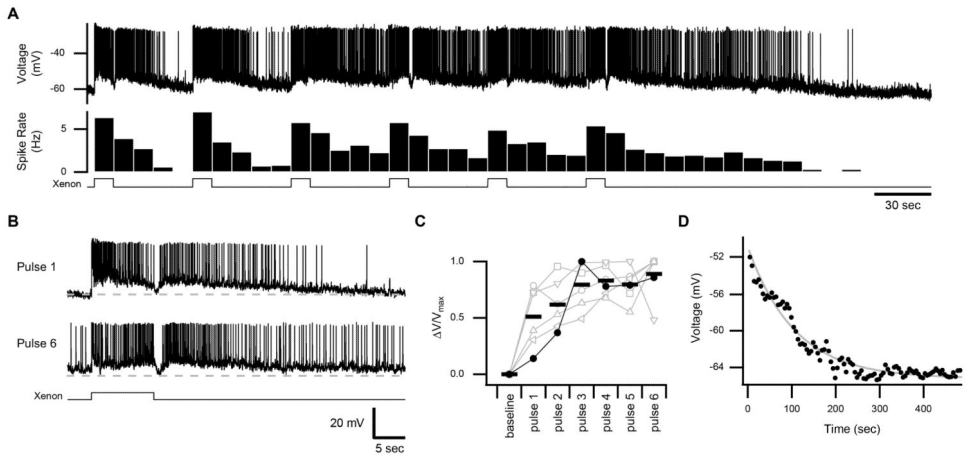

Figure 1. Persistent Responses and Temporal Integration of IpRGCs

(A) Membrane voltage of an ipRGC in response to a series of 10-sec pulses of white light (xenon at an intensity of 2.5×10^{-5} μW μm^{-2}, equivalent to 3.3×10^{4} lux). The corresponding spike rate is shown below in 10-sec bins. Light monitor at bottom. Activation that continues beyond the period of illumination is referred to as the persistent response. (B) Excerpts of the trace in A illustrating the response to the first and sixth light pulses. Dashed line represents the baseline (−60 mV). (C) Subthreshold membrane voltage, averaged from 30–40 sec after each light pulse, is displayed for individual cells (connected markers, n = 6 cells) and the population mean (bars) for this protocol. The difference from baseline, normalized to the maximum difference, is displayed for each cell. Closed markers represent the cell shown in A. (D) Subthreshold membrane voltage after the last pulse for the cell shown in A (in 5-sec bins). Time point 0 corresponds to the end of illumination. Fit is a single exponential (τ = 107 sec). All experiments were performed at 35 °C with synaptic transmission intact. See also Figure S1.

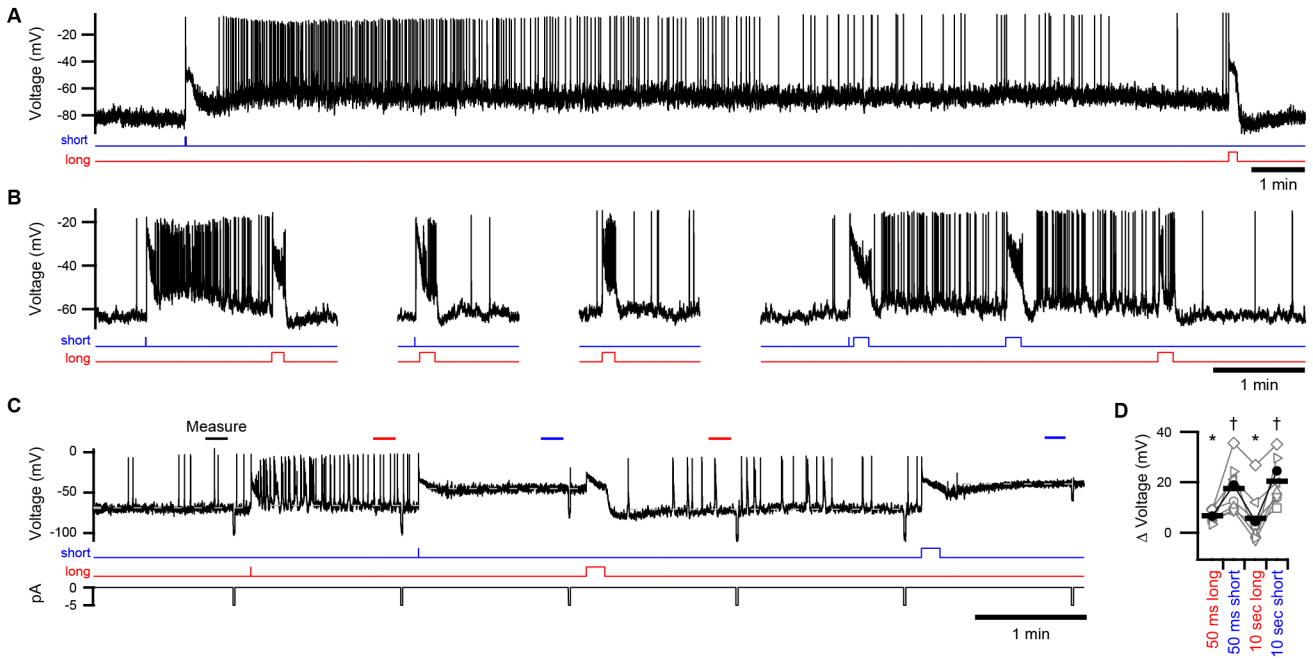

Figure 2. Persistent Responses are Inherent to IpRGCs and Bi-directionally Modulated by Light

(A) A persistent response evoked during pharmacological block of synaptic transmission. A flash of monochromatic, short-wavelength light was followed by darkness (~20 min) and then a pulse of long-wavelength light. (B) An example of wavelength- and timing-dependent modulations of the persistent response in another ipRGC. (C) Protocol for quantifying persistent responses in current clamp displayed with a representative recording. Periods of measurement are indicated by bars. Dashed lines indicate the average voltages measured following each stimulus (with lines extended for clarity). Persistent responses following short-wavelength stimuli are sufficiently large, in this cell, to cause depolarization block. Passive electrical properties were tested with hyperpolarizing current injections (5 pA, 1 sec; bottom trace). (D) Population data from the experiment illustrated in C with the difference in membrane voltage (from darkness) plotted for individual cells (connected markers) and the population mean (bars). Closed markers indicate the cell in C. Groups marked with asterisks and daggers differ significantly from each other ($n = 8$ cells, $p < 0.001$). All experiments were performed at 23 °C with synaptic transmission blocked. Light stimuli were 50-ms flashes or 10-sec pulses (monitors below traces). See Figure S2 for spectra and intensities of light.

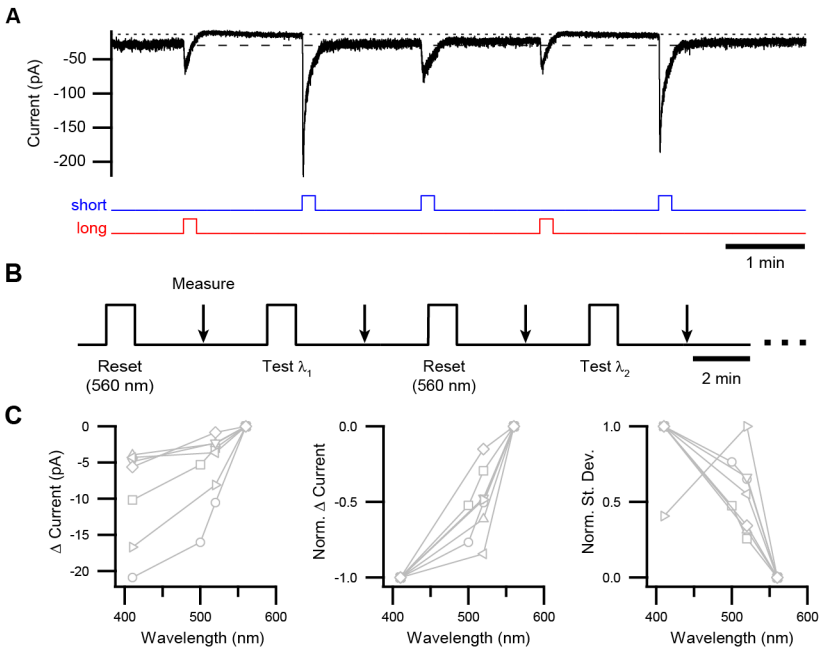

Figure 3. Wavelength-dependence of Persistent Responses Measured in Voltage Clamp

(A) Example of a persistent response (i.e., the light-evoked current that continues to flow beyond the period of illumination) modulated by successive pulses of short- and long-wavelength light. This response does not show temporal integration because it is saturated with each short-wavelength pulse at the intensity used here, and there is negligible dark regeneration between pulses. Light monitors shown below trace. See Figure S2 for spectra and intensities of light. (B) Protocol for quantifying the magnitude of the persistent response as a function of wavelength. Test wavelengths were alternated with a "reset" wavelength of 560 nm to establish a baseline. The intensities of all stimuli (1×10^9 – 2×10^9 photons μm^{-2} sec^{-1}) were sufficient to produce a saturated persistent response at each wavelength tested. (C) Population data from protocol in B for difference in current from baseline (left), difference in current normalized to minimum and maximum for each cell (middle), and current noise in the same period (standard deviation normalized to minimum and maximum; right). Connected markers are individual cells. All experiments were in voltage clamp (−80 mV) at 23 °C with synaptic transmission blocked.

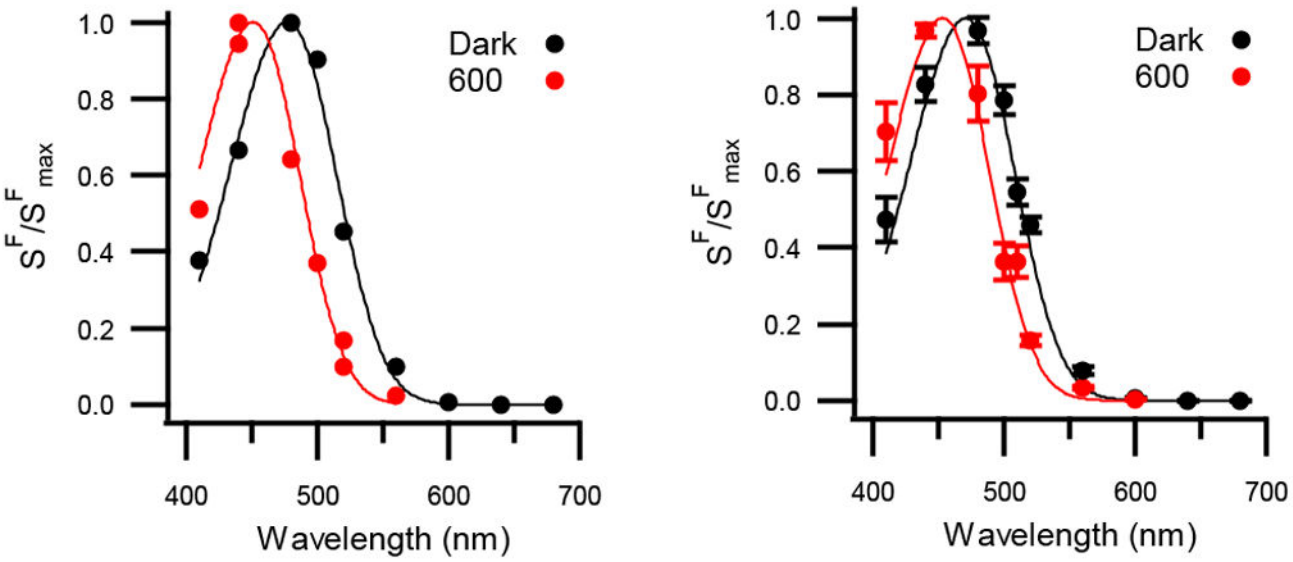

Figure 4. Two Silent States of Melanopsin Detected in IpRGCs

Left: The spectral sensitivity (i.e., action spectrum) of a single ipRGC measured in darkness as well as during a 600-nm background light (black and red markers, respectively). Plotted is the sensitivity of the cell to dim-flashes of each test wavelength (S^F, in pA photons^{-1} μm^2) normalized to the maximum for this cell (S^F_{max}). Continuous curves are single-state nomograms fit to the data with λ_{max} = 471 nm (darkness) and 454 nm (600-nm background). Right: Population averages for the same conditions (mean ± SEM; n = 6 cells) with λ_{max} = 471 nm (darkness, the "cyan" state) and 453 nm (600-nm background, the "violet" state). 600-nm background was delivered at 4×10^6 – 7×10^8 photons μm^{-2} s^{-1}. Measurements were made at 35 and 23 °C with no detectable variation in λ_{max} with temperature. Synaptic transmission was blocked and the holding voltage was −80 mV. See also Figure S3.

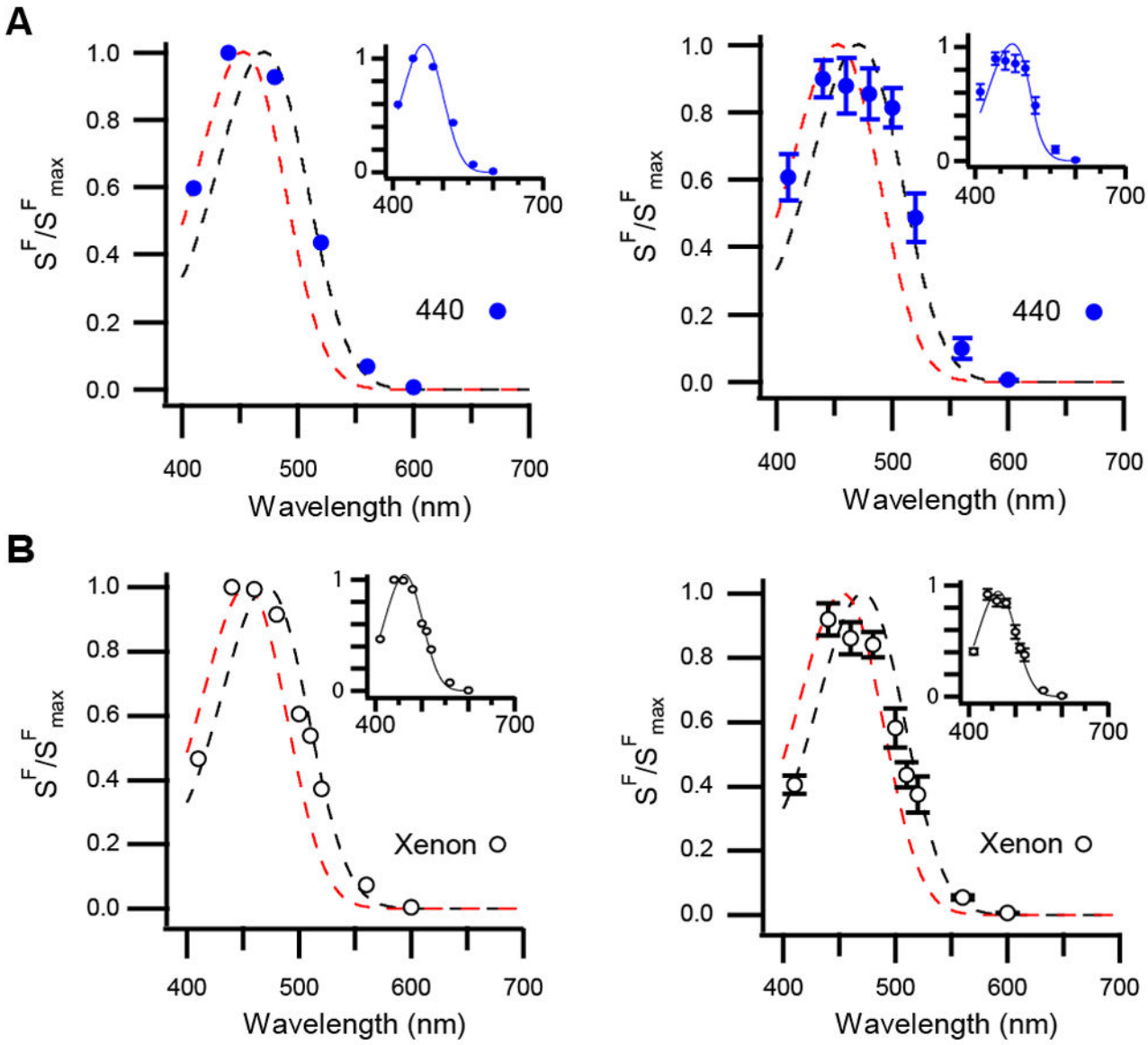

Figure 5. Broadened Spectral Sensitivity of IpRGCs Due to Activation of Melanopsin from Two Silent States

(A) Action spectrum of a single ipRGC (left) and the population (right) on a background of short-wavelength light (440 nm). Dashed lines are single-state nomograms used to fit the spectra in Figure 4 (black, representing the cyan state and red, the violet state). Insets: Same data but the curves are weighted sums of the same two nomograms (Left: 53% cyan and 47% violet; Right: 69% cyan and 31% violet). (B) Action spectrum measured from a single ipRGC (left) and the population (right) on a background of white (xenon) light. Black and red dashed lines represent the cyan and violet nomograms, respectively. Insets: same data but each curve is the weighted sum of the nomograms for the cyan and violet states (Left: 60% cyan and 40% violet; Right: 59% cyan and 41% violet). Background lights were 1×10^5 – 7×10^5 photons μm^{-2} sec^{-1} (440 nm) and 1.5×10^{-7} μW μm^{-2} (equivalent to 50 lux; xenon). Synaptic transmission was blocked. Experiments were performed at 35 and 23 °C, with no

difference between these conditions detected. Holding voltage was −80 mV. All error bars are SEM.

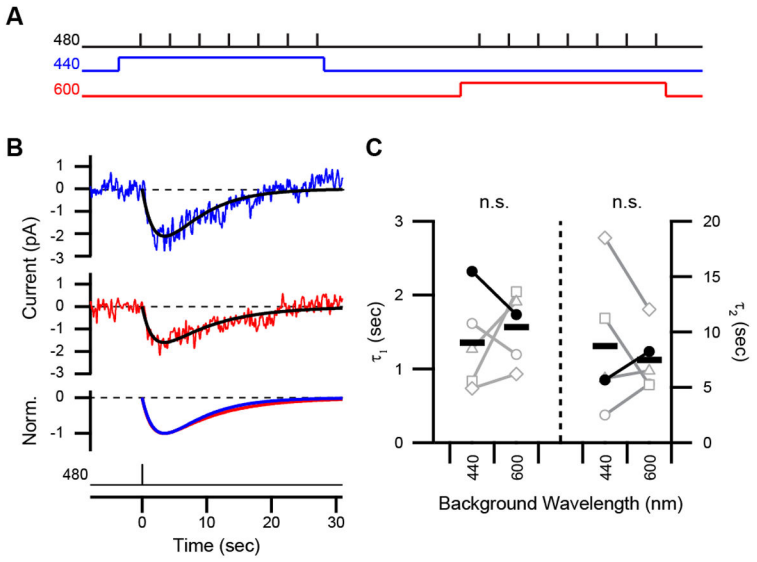

Figure 6. Indistinguishable Activation from the Two Silent States of Melanopsin

(A) Schematic of the protocol used to compare responses evoked from the cyan and violet states. A 440-nm background generates a majority fraction of the cyan state and a 600-nm background generates a dominant fraction of the violet state. Backgrounds were matched in intensity to produce equivalent activation of ipRGCs and presented in random order (3 and 2 cells with 440 and 600 nm first, respectively). (B) Dim-flash responses evoked on 440- and 600-nm backgrounds (blue and red traces, respectively). Traces are the average of seven trials. Fits are convolutions of two exponentials, $A\,(e^{-t/\tau 1} - e^{-t/\tau 2})$, shown normalized to their peaks in the bottom panel (time constants for blue and red traces: τ_1, 2.3 and 1.7 sec; τ_2, 5.7 and 7.5 sec). Light monitors are below. (C) Time constants from the population of cells (closed markers for the cell in B). "n.s." is lack of statistical significance. Background lights were 9×10^5 photons $\mu m^{-2}\ s^{-1}$ (440 nm) and 1×10^8 photons $\mu m^{-2}\ s^{-1}$ (600 nm). Synaptic transmission was blocked in all experiments, which were performed at 23 °C. Holding voltage was −80 mV.

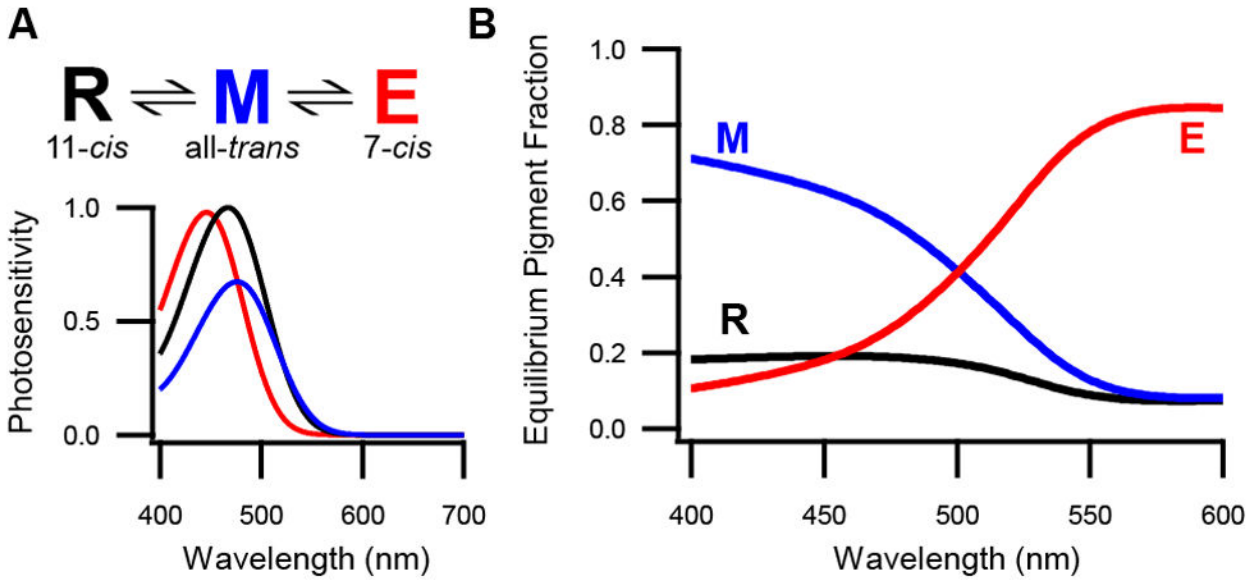

Figure 7. A State Model for Tristable Melanopsin

(A) State diagram of melanopsin (top) based on parameters measured biochemically from purified pigment (Matsuyama et al., 2012). Shown are melanopsin (R), metamelanopsin (M), and extramelanopsin (E) with chromophores designated. Below are plotted the relative photosensitivities (i.e., products of the extinction coefficients and quantum efficiencies) of these states as a function of wavelength. Only two model parameters are experimentally undefined: the quantum efficiency of the E state and the fraction of M isomerizations that yields the R versus E state (set at 0.4 and 0.5, respectively; Experimental Procedures). Only the latter parameter is not depicted here. Direct photoconversion between the R and E states is unlikely given energetic constraints of chromophore isomerization. (B) Predicted equilibrium fraction of each pigment state as a function of wavelength. Lines show the R state (black), M state (blue), and E state (red). See also Figure S4.

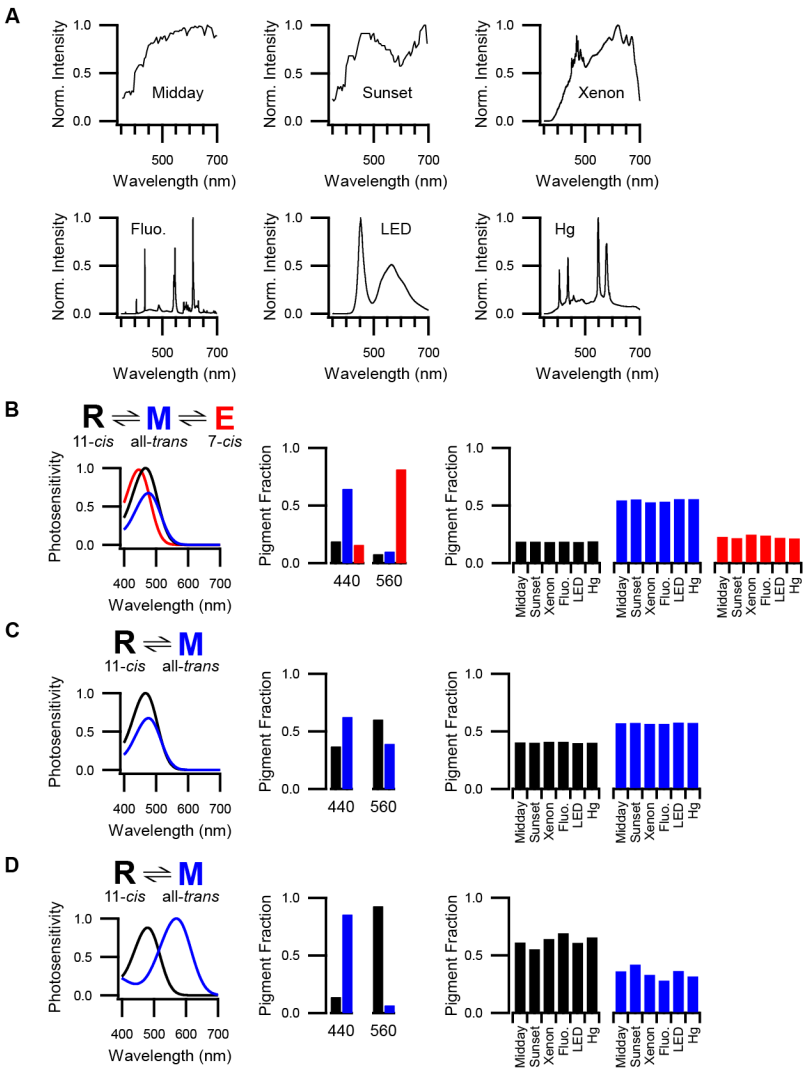

Figure 8. Melanopsin Tristability under Diverse Lighting Conditions

(A) Measured spectra of various, common light sources (in photons μm^{-2} sec^{-1} nm^{-1} prior to normalization). (B) Left: State diagram and relative photosensitivities as displayed in Figure 7A. Middle: Predicted equilibrium fractions of melanopsin states for monochromatic illumination at two wavelengths (440 and 560 nm). Right: Predicted equilibrium fractions of melanopsin states for broadband illumination by the sources shown in A. (C) Same as B but for a hypothetical bistable melanopsin with only the ground state (R) and metamelanopsin (M). (D) Same as B but for *Drosophila* rhodopsin (R) and metarhodopsin (M). Midday and sunset spectra in A are courtesy of Sönke Johnson (Johnsen et al., 2006).